Generation and Migration of Electrons and Holes during Naphthalene Sorption in Acidic Al-ZSM-5 Zeolites

Alain Moissette,*,† Hervé Vezin,‡ Isabelle Gener,§ and Claude Brémard†

Laboratoire de Spectrochimie Infrarouge et Raman UMR-CNRS 8516, Centre d' Etudes et de Recherches Lasers et Applications (FR-CNRS 2416), Bât. C5 Université des Sciences et Technologies de Lille, 59655 Villeneuve d'Ascq Cedex, France, Laboratoire de Chimie Organique et Macromoléculaire UMR-CNRS 8009, Bât. C3 Université des Sciences et Technologies de Lille 59655, Villeneuve d'Ascq Cedex, France, and Laboratoire de Catalyse en Chimie Organique, UMR-CNRS 6503, Université de Poitiers, 40 avenue du recteur Pineau, 80022 Poitiers, France

Received: April 11, 2003

In situ CW EPR, diffuse reflectance UV−visible and Raman scattering spectroscopies were used to monitor the spontaneous ionization of naphthalene by direct exposure to thermally activated acid HZSM-5 zeolite ($H_n(AlO_2)_n(SiO_2)_{96-n}$). Calcination of the zeolite is a prerequisite for the spontaneous ionization. It is shown through EPR and UV−visible results that the maximum yield of naphthalene radical cation $NPH^{\bullet+}$ increases gradually as the temperature of thermal treatment under O_2 increases and can reach 50%. The tight fit between the shape of $NPH^{\bullet+}$ and the pore size of straight channels of zeolites combined with aluminum content of zeolite appeared to be the most important factors responsible for the stabilization of the charge separation of naphthalene in $NPH^{\bullet+}$ and trapped electron. Complete disappearance as a function of time of $NPH^{\bullet+}$ with the persistence of paramagnetic species in high yield indicates that a supplementary electron-transfer reaction between $NPH^{\bullet+}$ and zeolite framework is taking place during the migration of $NPH^{\bullet+}$ and trapped electron. All the experimental data support the formation of positive holes within the zeolite framework stabilized by occluded NPH in ground state. The ZSM-5 zeolite participates as an electron donor in electron-transfer reaction with occluded $NPH^{\bullet+}$ preferentially to the direct charge recombination with trapped electron. The spontaneous initial charge separation evolves to long-lived charge separated state as an electron−hole pair. Deactivation of the long-lived electron−hole pair is observed over a long period at room temperature. The pulsed EPR results provide evidence of the fate of ejected electron and electron−hole pair as isolated electrons. This technique demonstrates interaction between isolated electron and ^1H and ^{13}C nuclei of occluded naphthalene. Unfortunately, no evidence was found for interaction of unpaired electron with ^{27}Al and ^{29}Si nuclei of zeolite framework as previously described for analogous system using biphenyl.

Introduction

Charge separation (CS) over nanometer distances in artificial arrays is a topic of high relevance for both fundamental and applied chemical sciences. Charge separated state (CSS) is the most fundamental energy conversion process of photovoltaic effect, exciton storage in semiconductors, as well as photosynthesis.[1]

Charge separation can be induced by different ways using radiations such as fast electrons, γ-ray, X-ray, far-UV light, or visible light. However, the investigations to study the CSS are hampered by the fact that often charge recombination (CR) occurs rapidly. For the production of artificial molecular systems where both the long-distance charge transport and the formation of the long-lived CSS are possible, molecular sieves such as zeolites have often been employed as prototypical organizing media. Zeolites are crystalline aluminosilicates possessing an open framework of molecular-sized pores. Many molecules are readily sorbed within this microporous network. The regular periodic array of void spaces throughout the zeolite crystal, typically several μm in size, facilitates the spatial arrangement of thousands of molecules with significant long-range ordering. The photoinduced single-electron transfer (PET) of occluded molecules initiates further migration of electrons and holes within the zeolite framework leading to long-lived CSS.[2−5] Different mechanisms are proposed to explain long or short transfer of electrons and holes through zeolite framework.

Surprisingly, the mere exposure of electron donor or electron acceptor compounds to activated zeolites can initiate spontaneous CS through single-electron transfer (ET) with zeolite host.[6−9] Often, the formation of hydrocarbon deposits (coke) during the reaction of hydrocarbon on acid zeolites was previously reported.[10,11]

Recently, we have reported that the spontaneous CCS was observed even at least 1 year after sorption of biphenyl in activated acidic ZSM-5 zeolites. After a primarily ionization of biphenyl in radical cation and electron, effective charge transports were postulated for the formation of the long-lived electron−hole pairs as CSS and decrease in the CR rate. The electron and positive hole appear separated by the occluded biphenyl and efficiently trapped in the neighboring side pockets of the straight channel of ZSM-5 zeolite. However, the CSS yield was weak and many uncertainties about the generation and migration of electrons and holes remain.[12,13]

In this work, we employ electron paramagnetic resonance (EPR) spectroscopy, diffuse reflectance UV−visible absorption

* Address correspondence to this author. Fax: 33(0)320436755; e-mail: alain.moissette@univ-lille1.fr.

† Laboratoire de Spectrochimie Infrarouge et Raman, Université de Sciences et Technologies de Lille.

‡ Laboratoire de Chimie Organique et Macromoléculaire, Université de Sciences et Technologies de Lille.

§ Laboratoire de Catalyse en Chimie Organique, Université de Poitiers.

10.1021/jp034976k CCC: $25.00
Published on Web 07/18/2003

spectroscopy, and multiexcitation Raman spectroscopy to investigate extensively the generation and migration of electrons and holes in acidic ZSM-5 zeolites through sorption of naphthalene (NPH). Applying pulsed EPR techniques, we were able to characterize the surroundings of unpaired electron species of an unusual long-lived electron hole pair in high yield.

Experimental Section

Materials. As-synthesized ZSM-5 samples (Si/Al = 13.5, 27, particle size 2 μm) were obtained from VAW aluminum (Schwandorf, Germany). Crystals of silicalite-1 (Si/Al > 1000) and Al-ZSM-5 (Si/Al ~31, particle size 5 μm) were synthesized in high purity according to the fluoride medium procedure in the Laboratoire des Matériaux Minéraux, UMR-CNRS 7016, ENSC Mulhouse. EPR spectroscopic investigations indicate iron impurities at trace levels in the industrial zeolites not detected by conventional elemental analyses. All the zeolite samples were used after a calcination procedure under O_2 or Ar at 773 K without other indication. The thermal treatment removed completely the water content and the template of the as-synthesized zeolites. The unit cell composition of the calcined H_n-ZSM-5 samples were $H_{3.0}(AlO_2)_{3.0}(SiO_2)_{93.0}$ (Si/Al = 31); $H_{3.4}(AlO_2)_{3.4}(SiO_2)_{92.6}$ (Si/Al = 27); and $H_{6.6}(AlO_2)_{6.6}(SiO_2)_{89.4}$ (Si/Al = 13.5) from elemental analysis. The powder XRD patterns, ^{29}Si, ^{27}Al MAS NMR, IR absorption, and Raman spectra of bare ZSM-5 zeolites are well-documented. The powder XRD patterns and spectra of the samples under study correspond to the expected phases of these porous materials. However, the ^{27}Al NMR spectra of hydrated $H_{6.6}$ZSM-5 (Si/Al = 13.5) sample provide evidence of small amount of extraframework hexacoordinated Al species. The Brønsted and Lewis acidity of the samples were characterized by FTIR measurements using pyridine as probe molecule.

Naphthalene (NPH,$C_{10}H_8$, Merck-Schuchardt) was purified by sublimation and stocked over molecular sieves. Pure and dry Ar and O_2 gas were used.

Sorption of Naphthalene in Acidic ZSM-5. Weighted amounts (~1.4 g) of powdered hydrated zeolite $H_n(AlO_2)_n(SiO_2)_{96-n}$ were introduced into an evacuable heatable silica cell. The sample was dried under vacuum (10^{-3} Pa) and heated stepwise to 773 K under O_2 without other indication. The crystallinity of the samples was checked by XRD and was not reduced by this treatment. Then, the sample was held under vacuum and cooled to room temperature under dry argon. Weighted amounts of NPH corresponding to 0.5, 1, 2, 3, or 4 molecules per unit cell (UC) were introduced into the cell under dry Ar and the powder mixture was shaken. The powders were transferred under dry argon in a quartz glass Suprasil cuvette for Raman and diffuse reflectance UV−visible experiments or in cylindrical EPR quartz tube.

Chemical Extraction of Stable Products Occluded in Acidic ZSM-5. $H_n(AlO_2)_n(SiO_2)_{96-n}$ zeolite samples loaded with 1 or 2 NPH/UC were suspended in HF solution. After slow gentle warming of the mixture, the organic compounds were extracted by hexane after complete destruction of the zeolite framework. The gas chromatographic analysis was used to detect and quantify organic compounds.

Instrumentation. The UV−visible absorption spectra of the sample were recorded between 200 and 800 nm using a Cary 3 spectrometer. The instrument was equipped with an integrating sphere to study the powdered zeolite samples through diffuse reflectance; the corresponding bare zeolite was used as the reference. The DRUVv spectra were plotted as the Kubelka−Munk function: $F(R) = (1 - R)^2/2R = K/S$, where R represents the ratio of the diffuse reflectance of the loaded zeolite to that of the dehydrated neat zeolite, K designates an absorption coefficient proportional to the concentration of the chromophore, and S represents the scattering coefficient of the powder.

In situ FTIR spectra were recorded in the region 4000−400 cm^{-1} on a Nicolet 730 spectrometer, using a homemade cell and thin self-supported wafers (8−10 mg/cm^2). The spectra were recorded with a resolution of 2 cm^{-1} using 200 scans. The cell was connected to an evacuation gas flow system, which allowed thermal treatment up to 773 K. The zeolite wafers were first calcined overnight in O_2 and then evacuated under vacuum for 1 h at 773 K. The spectra were recorded before, after pyridine absorption and after evacuation of pyridine. The Brønsted acid sites of ZSM-5 will protonate pyridine, forming the pyridinium ion, which has a characteristic ring vibrational frequency at 1545 cm^{-1}. Lewis aluminum being an electron pair acceptor can bind pyridine in a covalent fashion, giving rise to a vibrational band at 1465 cm^{-1}. The relative amounts of Brønsted and Lewis aluminum can be estimated by integration of these two bands after correction for differences in IR absorption cross sections.

Raman scattering spectra were collected on a Kaiser spectrometer equipped with a Peltier-cooled charge coupled device detector. The excitation wavelength used was 632.8 nm with low power at sample. The laser line was supplied by helium−neon laser. The spectrometer calibration was verified using the Raman lines of silicon. This resulted in an accuracy of less than ±1 cm^{-1}. A Bruker IFS 88 instrument was used as a near-IR FT-Raman spectrometer with a CW Nd:YAG laser at 1064 nm as excitation source. A laser power of 100−200 mW was used. The spectra (3500−150 cm^{-1}) were recorded with a resolution of 2 cm^{-1} using 600 scans. The Opus Bruker software was used for spectral acquisition, data treatment, and plotting.

The CW X-band EPR spectra were recorded between 500 and 100 K on a Bruker ELEXYS 580-FT spectrometer. The EPR spectra were double integrated using Bruker software and the spin concentration was determined relative to a reference standard. This standard sample is calcined $H_{3.0}(AlO_2)_{3.0}(SiO_2)_{93.0}$ zeolite loaded with different nitroxide amounts (3-carbamoyl-2,2,5,5-tetramethyl-3-pyrrolin-1-yloxy, free radical, 99%, Aldrich). All pulsed EPR experiments were performed on a Bruker ELEXYS 580-FT spectrometer at low (4.2 K) and room temperature. The two pulse spin−echo correlation spectroscopy (SECSY) was achieved using Pulse Spel program with the following sequence: $\pi/2-t_1-\pi/2-t_1-t_2$. A 12 ns $\pi/2$ pulse width allowed sufficient wide band coverage. The initial t_1 was set up at 120 ns because of spectrometer dead time and 256 steps along t_1 were used with t_1 step size of 16 ns. Then, fourth order baseline correction was applied and Hamming apodization was performed along both t_1 and t_2 directions prior to 2D Fourier transformation and magnitude calculation. The HYSCORE measurements were carried out with the sequence $\pi/2-\tau-\pi/2-t_1-\pi-t_2-\pi/2-\tau$ echo and a four-step phase cycle. The pulse lengths of the $\pi/2$ and π pulses in these experiments were 12 and 24 ns, respectively. The HYSCORE experiments were recorded with t value of 256 ns leading to a t_1 suppression effect for ^{1}H and ^{13}C patterns. Prior to Fourier transformation of the HYSCORE data, the background decay was removed by a polynomial fit and apodized with a Hamming function. Absolute value of the 2D FFT is performed.

The data processing of UV−visible absorption spectra recorded during the sorption was performed using the SIMPLISMA (SIMPle-to-use Interactive Self-modeling Mixture Analysis) approach.[14] This method was applied to extract the characteristic spectra of species generated through sorption from

many spectral data. SIMPLISMA resolves spectrum of mixture into pure component spectra without any prior information. In addition, the program calculates the relative concentration of the species. The accuracy of the calculation is given by residuals which represent the difference between the reconstructed and the original data. This coefficient can be seen as a standard deviation and was defined previously.[14,15] The values range between 0 and 1. The algorithm for SIMPLISMA calculation was detailed elsewhere.[14,15,16]

The molecular modeling were performed on a Silicon Graphics workstation using Cerius^2 (version 3.8) package from Molecular Simulations Incorporation. The zeolite structural parameters, force field, and calculation details used to carry out the minimization procedure of the nonbonding energy were previously described.[17] The structural parameters and set of atomic charges of the guests were derived from previous structural and theoretical works.[18]

Results

Characterization of Activated H_nZSM-5 Zeolites. The framework structure of ZSM-5 zeolites contains two types of intersecting channels, both formed by rings of 10 oxygen atoms, characterizing them as a medium-pore zeolite.[19−21] One channel type is straight and has a nearly circular opening (0.53 × 0.56 nm), while the other one is sinusoidal and has an elliptical opening (0.51 × 0.55 nm). These channels are sufficiently wide to allow NPH molecules to pass through openings of channels to be occluded at the channel intersection of silica rich H-ZSM-5 zeolite (Si/Al = 300).[22] After calcination at 773 K under O_2 or Ar of zeolites (Si/Al ∼30) and subsequent rehydration, no extraframework aluminum species were detected by ^{27}Al MAS NMR spectroscopy. However, the hydrated sample with framework ratio Si/Al = 13.5 exhibits a significant amount of extraframework aluminum, represented as 0.2 Al_2O_3 per unit cell as deduced by ^{27}Al MAS NMR measurements and chemical analysis.

Brønsted acid sites (BAS) are assigned to bridging hydroxyl groups Al−OH−Si. So far, the problem of locating the Al atoms and associated proton or deuterium in H(D)-ZSM-5 by X-ray or neutron diffraction techniques was not resolved. However, numerous theoretical and experimental investigations provide significant findings about the distribution, structure, and acid strength of Brønsted acid sites of H-ZSM-5 zeolites with Si/Al ratio corresponding to samples under study.[23,24] The Brønsted acid sites of the calcined zeolite samples under study were characterized by IR absorption spectra in the OH stretching region. In the spectra of all samples calcined at 773 K under Ar or O_2, a strong band at 3610 cm^{-1} (Si/Al = 27) or 3612 and 3605 cm^{-1} (Si/Al = 13.5) because of the bridged OH was detected, while a low intensity band can be seen at about 3737 cm^{-1} which can be attributed to silanol group. The OH stretching vibrations associated with extraframework aluminum species (around 3700, 3670, and 3525 cm^{-1}) were not detected. It was previously demonstrated that the IR absorption in the OH stretching region decreases and broadens markedly after activation at higher temperature particularly under O_2, such trends were observed with the present zeolite samples.[25] Numerous papers and reviews have been published about the IR spectroscopy measurements of adsorption of probe molecules such as pyridine, ammonia, and acetonitrile to study the acidity of zeolites.[26,27]

Evidence of Lewis acid sites (LAS) which are essentially electron acceptor centers was previously reported in activated acidic ZSM-5.[28] The structure of Lewis sites is still controversial. Some authors associate LAS with trigonal Al atoms formed as a result of zeolite dehydroxylation by thermal treatment. Other research groups have proposed Al^{3+} species or various other nonframework species (AlO^+, $Al(OH)^{2+}$, $Al(OH)_3$, AlO(OH), Al_2O_3, etc.) leached from the zeolite framework during chemical or thermal treatment. The exact nature of these species is, however, still unknown.[28] The relative amounts of Brønsted and Lewis aluminum of activated H_nZSM-5 (n = 3.4, 6.6) zeolites were estimated by integration of the IR bands observed at 1545 and 1465 cm^{-1} after sorption of pyridine. The LAS amounts were 0.4/UC and 0.2/UC for $H_{6.6}$ZSM-5 and $H_{3.4}$ZSM-5 zeolites dehydrated under O_2 over 24 h at 773 K. These relative amounts decrease markedly after dehydration under Ar whereas they increase with temperature of calcination under O_2 between 573 and 973 K. However, the amounts of LAS remain low. These LAS are not thought to be inherent to the ZSM-5 structure but are probably generated during calcination, resulting in partial breaking of Al−O bonds. The low amounts of extraframework Al compounds induce weak effect upon the LAS.[29] It was demonstrated previously by EPR diagnostic of NO sorption that the Lewis acidity of ZSM-5 zeolites increases markedly as a function of the calcination temperature under O_2 between 600 and 1000 K whereas the nonframework Al content has a weak effect on the Lewis acidity. EPR of sorbed NO in zeolites is probing LAS strong enough to quench the orbital moment of NO molecule.[28] No such experiments were carried out on the zeolite samples used in this study.

CW EPR Investigations of Naphthalene Sorption in Calcined H_nZSM-5 Zeolites. The commercial forms of aluminated H_nZSM-5 zeolites activated at 773 K under O_2 or Ar after evacuation under vacuum and subsequent admission of Ar gave rise to very weak EPR signals with g = 4.26 at 100 or 300 K. This feature is absent for samples of silicalite-1 (Si/Al > 1000) and Al_3-ZSM-5 (Si/Al ∼31) synthesized in high purity according to fluoride medium procedure. This signal observed in commercial samples was assigned to Fe(III) impurities at trace levels. No signal was detected for g-values around 2.[30] No supplementary signal was detected for silicalite-1 (Si/Al > 1000) activated under Ar or O_2 and loaded by NPH (1 NPH per unit cell) in our experimental conditions.

Weak features were observed in the 2 g-values for aluminated H_nZSM-5 (n= 3.4, 6.6) zeolites calcined at 773 K under Ar and loaded by NPH (1 NPH/UC). In contrast, intense signal was observed immediately after mere exposure under Ar of solid NPH to aluminated H_nZSM-5 (n = 3, 3.4) samples calcined under O_2 at 773 K, Figure 1. Numerous EPR spectra were recorded at different times during NPH sorption in $H_{3\cdot4}$ZSM-5, Figure 1. The empty zeolite sample was completely evacuated under vacuum before the introduction of solid NPH under argon. The X-band EPR spectra exhibited the characteristic features of previously reported $NPH^{\bullet+}$ spectrum. The characteristic spectral line shape is caused mainly by the hyperfine anisotropy of the ring protons.[31]

In addition to narrow lines, the EPR spectra contain broad overlapping feature which increases in intensity during the sorption, Figure 1. The data processing using the SIMPLISMA approach of the spectra set provides evidence of two spectra. Analogous phenomena were observed previously during the sorption of o-chloranyl within cesium modified X and Y zeolites and during the sorption of biphenyl in activated H_nZSM-5.[32,33] One spectrum (A) with resolved hyperfine structure was readily assigned to $NPH^{\bullet+}$, whereas the other one (B) with broad structureless signal was tentatively attributed to isolated electrons. The possibility of electron trapping by H^+ of Si−OH−

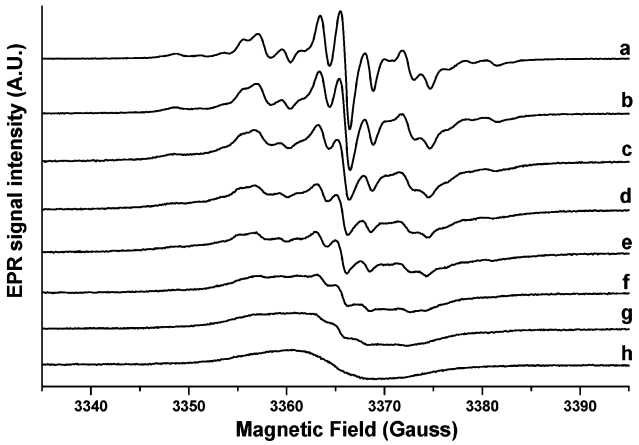

Figure 1. EPR spectra recorded at room temperature during the sorption of naphthalene in H_3ZSM-5 $[H_3(AlO_2)_3(SiO_2)_{93}]$ zeolite activated at 773 K under O_2. (a) 15 min after the mixing of the powders, (b) 6 h, (c) 1 day, (d) 3 days, (e) 1 week, (f) 2 weeks, (g) 1 month, and (h) 2 months.

Al group can be ruled out.[34] The double integration of A and B signals provides spin density values as a function of time. The spin density was expressed in spins per unit cell. Figure 2 exhibits the spin density corresponding to A and B components detected over 1 day after the exposure at room temperature of solid NPH to H_3ZSM-5 activated at 773 K under O_2.

From Figure 2, one can observe that A and B intensities are practically equivalent 30 min after the mixture of solids and correspond to 0.14 spin/UC. The $NPH^{\bullet+}$ signal decreases to 0.06 spin/UC during the first 3 h and reaches a plateau at 0.05 in about 6 h. In contrast, the broad signal increases markedly from 0.12 to 0.33 spin/UC during the first 5 h and increases to 0.38 spin after 24 h. At room temperature, the disappearance of $NPH^{\bullet+}$ goes to zero over 1 month after the mixing of the solids, whereas the broad signal is still prominent after several months. Upon heating at 400 K of equilibrated sample at room temperature (24 h), the disappearance of $NPH^{\bullet+}$ was complete over 6 h whereas the broad signal decreases from 0.48 to 0.24 over the same period and goes to zero over several days at 400 K, Figure 2. Cooling to room temperature stopped the decrease of the signal and trapped the paramagnetic moieties within the zeolite framework.

In the same way, numerous EPR spectra were recorded at different times during NPH sorption in $H_{6.6}ZSM-5$ activated at 773 K under O_2, with a loading corresponding to 1 NPH/UC. The EPR results (not shown) were qualitatively analogous at room temperature and 400 K to that described above. The maximum values of $NPH^{\bullet+}$ (A signal) and electron and hole (B signal) spin densities measured by CW EPR measurements during the NPH sorption are listed in Table 1 according to the calcination and loading conditions of the H_nZSM-5 zeolites. The complete exchange of H^+ by Na^+ and calcination under O_2 does not lead to any ionization of NPH through sorption in Na_nZSM-5 zeolites (n=3.4, 6.6). No significant difference was observed between the maximum values of A and B spin density yields corresponding to $H_{3.4}ZSM-5$ commercial and H_3ZSM-5 high purity samples, Table 1. Apparently, the iron impurities at trace levels have no effect upon the ionization of NPH. The maximum density of spin of $NPH^{\bullet+}$ (A signal) generated by sorption depends highly on the temperature of calcination under O_2 and on the calcination time. The ionization yield can reach 30% of occluded NPH after thermal treatment of $H_{6.6}ZSM-5$ over several days under O_2 at 873 K. It is difficult to estimate the maximum of spin density of the electrons and holes (B signal)

TABLE 1: Maximum Spin Densities Per Unit Cell (UC) of Radical Cation $NPH^{\bullet+}$, Ejected Electrons, and Holes Components Detected as a Function of Zeolite Type, Thermal Treatment under O_2 Atmosphere and Naphthalene Loading

zeolites	calcination O_2, (T °K)	NPH loading NPH/UC	$NPH^{\bullet+}$ spin/UC	electron−hole spin/UC
silicalite-1	773	1	0	0
$H_{3.4}ZSM-5$	473	1	0.01	0.07[a]
$H_{3.4}ZSM-5$	573	1	0.05	0.20[a]
$H_{3.4}ZSM-5$	673	1	0.09	0.43[a]
$H_{3.4}ZSM-5$	773	1	0.14	0.48[a]
H_3ZSM-5	773	1	0.12	0.42[a]
$H_{3.4}ZSM-5$	873	1	0.16	0.50[a]
$H_{3.4}ZSM-5$	973	1	0.19	0.56[a]
$H_{3.4}ZSM-5$	773	1	0.12	∼0.2[b]
$Na_{3.4}ZSM-5$	773	1	0	0
$H_{6.6}ZSM-5$	773	0.5	0.07	0.09[c]
$H_{6.6}ZSM-5$	773	1	0.10	0.21[c]
$H_{6.6}ZSM-5$	773	2	0.20	0.18[c]
$H_{6.6}ZSM-5$	773	4	0.10	0.16[c]
$H_{6.6}ZSM-5$	873[d]	1.5	0.50	
$H_{6.6}ZSM-5$	773	1	0.11	0.48[b]
$Na_{6.6}ZSM-5$	773	1	0	0

[a] sample heated at 400 K. [b] One year at room temperature. [c] zeolite with extraframework cations. [d] Long-time calcination procedure.

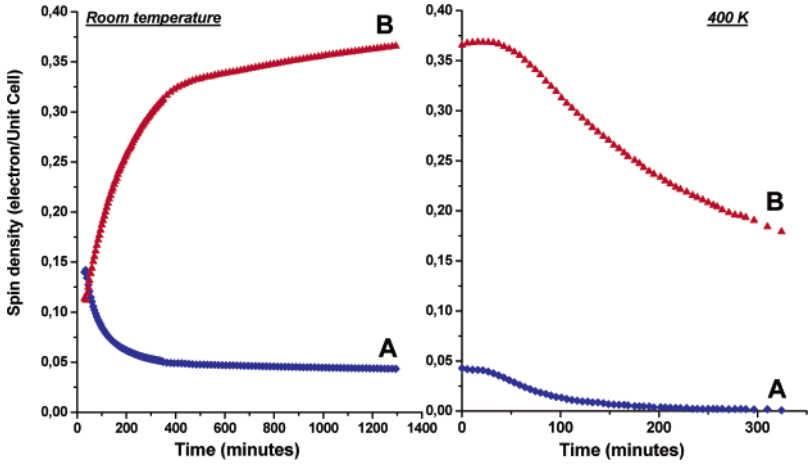

Figure 2. Spin densities corresponding to $NPH^{\bullet+}$ (A) and to unpaired electrons and holes (B) components detected as a function of time. Left: over 1 day after the exposure at room temperature of solid NPH to H_3ZSM-5 activated at 773 K under O_2. Right: upon heating at 400 K of the equilibrated sample at room temperature (24 h).

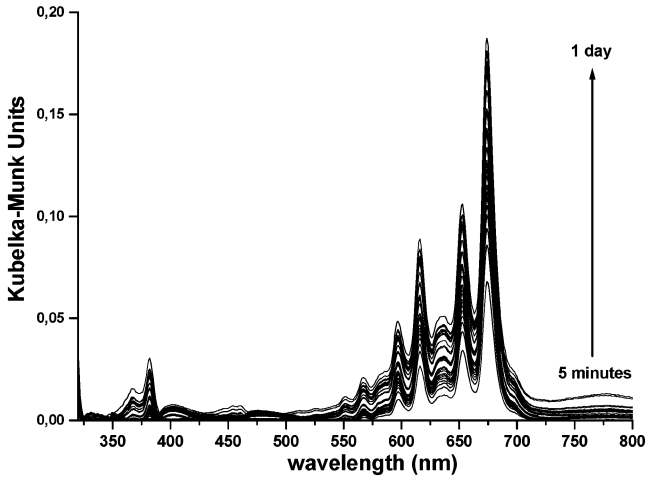

Figure 3. DRUVv spectra recorded at room temperature during the sorption of NPH in $H_{3.4}$ZSM-5 [$H_{3.4}(AlO_2)_{3.4}(SiO_2)_{92.6}$] zeolite activated at 773 K under O_2 in the 320−800 nm spectral range.

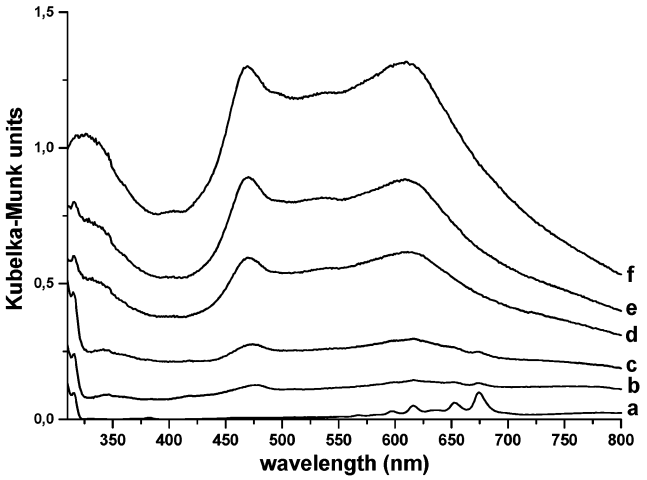

Figure 4. DRUVv spectra recorded for different time (b, c, d, e, f) under heating at 400 K of a sample (a) obtained 24 h after the mixing of NPH (1 NPH/UC) with $H_{3.4}$ZSM-5 calcined at 773 K under O_2.

generated at room temperature because of the slowness of the migration of electrons and holes (CSS) and competitive CR. The maximum of CSS spin density is better determined after gentle warming at 400 K and reaches 0.5/UC starting from 0.15/UC of $NPH^{\bullet+}$. The spontaneous ionization rate and yield (CS) increase as the calcination temperature increases. In the same way, the electron−hole pair (CSS) yield increases as the ionization yield (CS) increases. Finally, complete charge recombination (CR) occurs over several days at 400K.

Diffuse Reflectance UV−Visible Absorption Study of Naphthalene Sorption in Calcined H_nZSM-5 Zeolites. NPH and calcined H_nZSM-5 ($n = 0$, 3.4, 6.6) powders are colorless. No color was observed after the mixture of NPH with H_nZSM-5 dehydrated under Ar at 573 K. In contrast, several minutes after the mixing of solid NPH with H_nZSM-5 (n= 3.4, 6.6) zeolites calcined at 773 K under O_2, the powder turned blue. No such color was observed after mixture of NPH and silicalite-1 ($n = 0$) calcined in the same experimental conditions. Several months at room temperature after mixing, the blue powder turned to dark pink. Analogous dark pink powders were obtained after several days under gentle warming (400 K).

DRUVv spectra (not shown) recorded during 1 day after the mixing of NPH with silicalite-1 ($n = 0$) calcined under O_2 at 773, 873, or 973 K exhibit marked increasing of the prominent band at 270 nm. This feature was attributed to sorption of NPH in the ground state within the void space of porous material. Analogous results were observed after mixing of solid NPH with H_nZSM-5 dehydrated at 573 K under Ar. In contrast, the DRUVv spectra recorded during 1 day after the mixing of solid NPH with H_nZSM-5 zeolites ($n = 3.4$, 6.6) calcined at 673, 773, and 873 K under O_2 exhibit supplementary absorption bands.

Figure 3 shows some of the DRUVv spectra recorded at room temperature after the mixing of NPH (1 NPH/UC) with $H_{3.4}$-ZSM-5 calcined at 773 K. The most characteristic features of the spectra are very sharp bands between 550 and 680 nm with other absorptions at 350 and 385 nm. These supplementary spectral features were straightforward assigned to $NPH^{\bullet+}$ by comparison with previous UV−visible investigations of $NPH^{\bullet+}$ trapped in solid Ar.[35−37]

The characteristic absorption bands of $NPH^{\bullet+}$ of all the samples disappeared approximately after one month at room temperature with concomitant appearance of ill-defined large and broad bands in the visible region. After several months at room temperature, the shape of the bands broadened to large background with maximum in the red region.

Figure 4 shows some of the DRUVv spectra recorded under warming at 400 K of a sample obtained 24 h after the mixing of NPH (1 NPH/UC) with $H_{3.4}$ZSM-5 calcined at 773 K under O_2. The broad absorption bands obtained after the disappearance of the $NPH^{\bullet+}$ bands were assigned to unpaired electrons of electron−hole pairs (CSS) generated by electron transfer between $NPH^{\bullet+}$ and the zeolite framework by comparison with previous works.[38] Finally, after several days under gentle warming, the UV−visible absorption spectra were analogous to spectra recorded after the complete sorption of NPH in acidic H_nZSM-5 dehydrated at 573 K under Ar with very weak ionization.

To unequivocally assign specific absorption and to provide concentration dependence over time of the absorbing species, data processing of the DRUVv spectra sets were recorded over a long period after the mixing was carried out. The Simple-to-used Interactive Self-modeling Mixture Analysis (SIMPLISMA) program was used. A spectrum with a prominent band around 270 nm was resolved for all the spectra sets. It was assigned to NPH occluded in the void space of H_nZSM-5 zeolites ($n = 0$, 3.4, 6.6). For all the aluminated zeolites activated under O_2, a $NPH^{\bullet+}$ spectrum with characteristic narrow bands at 308, 367, 382, 445, 453, 460, 510, 525, 551, 567, 580, 585, 597, 616, 632, 637, 653, and 674 nm was resolved, Figure 5a.[35−37]

No evidence was found for the dimer cation radical as well as the radical anion.[39,40] The narrow bands of $NPH^{\bullet+}$ is a vibronic band system as obtained in solid Ar matrix. Particularly, three vibrational intervals can be distinguished in the $^2B_{3g} \leftarrow {}^2A_u$ electronic transition observed at 674 nm. The first interval was 1420 cm^{-1}, the second interval was 505 cm^{-1}, and the third interval was 800 cm^{-1}.[35−37] For H_nZSM-5 zeolites ($n = 3.4$) calcined under O_2, in addition to $NPH^{\bullet+}$ spectrum, two supplementary spectra were resolved from spectra sets recorded at room temperature during the sorption of NPH. The first one with absorption bands at 320, 400, and 480 nm (Figure 5c) was tentatively assigned to ejected electron (CS) associated with $NPH^{\bullet+}$ whereas the second one with broad bands around 500 and 750 nm (Figure 5b) was assigned to unpaired electrons of electron−hole pairs (CSS) by comparison with previous works devoted to biphenyl.[12,13,33,38]

For aluminum rich $H_{6.6}$ZSM-5 zeolite calcined under O_2, only one spectrum with broad bands around 500 and 750 nm was resolved in addition to $NPH^{\bullet+}$ spectrum. This spectrum was

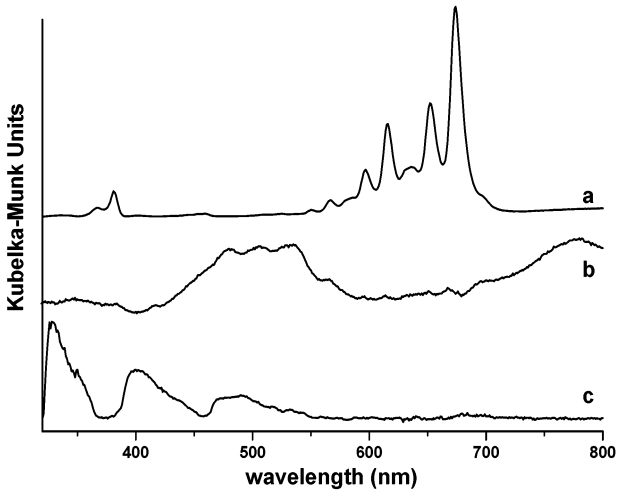

Figure 5. Pure DRUVv spectra extracted using the SIMPLISMA method of the DRUV data recorded during the sorption of naphthalene into $H_{3.4}(AlO_2)_{3.4}(SiO_2)_{92.6}$: (a) $NPH^{\bullet+}$; (b) electron−hole pair; (c) ejected electron.

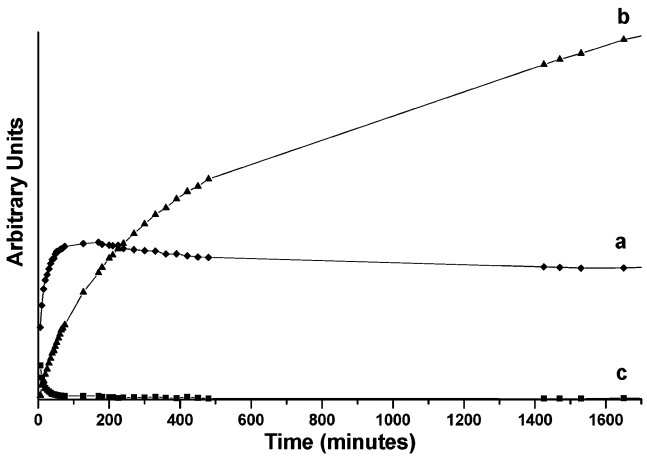

Figure 6. Relative contribution as a function of time of pure species deduced from the SIMPLISMA method from the DRUVv spectra recorded during the sorption of naphthalene into $H_{3.4}(AlO_2)_{3.4}(SiO_2)_{92.6}$: (a) $NPH^{\bullet+}$; (b) electron−hole pair; (c) ejected electron.

straightforward attributed to unpaired electrons of electron−hole pairs. No evidence of supplementary spectrum with bands at 320, 400, and 480 nm assigned to ejected electron in its trapping site was found using the SIMPLISMA approach.

The SIMPLISMA program provides also the relative concentration of species corresponding to resolved spectra as a function of time with respect to the UV−visible absorption cross sections. For example, Figure 6 shows the relative amounts of $NPH^{\bullet+}$ and trapped electron and electron−hole pairs observed over 1 day through the concentration associated with the resolved spectra exhibited in a, c, and b curves of Figure 5, respectively.

Figure 6 concerns the sample obtained after the mixing at room temperature of NPH with $H_{3.4}$ZSM-5 calcined at 773 K with 1 NPH/UC loading. Curve a in Figure 6 indicates the appearance of $NPH^{\bullet+}$ over 100 mn and a very weak decrease in concentration over 1600 mn. Concomitantly, the concentration of trapped ejected electron (Figure 6c) increases and decreases to zero over 100 mn whereas the electron−hole pair (Figure 6b) increases progressively in concentration over 1600 mn. Analogous trends were obtained with all the samples. However, as noted above, the trapped electron ejected during the primary ionization of NPH was not detected in experiments with aluminum rich $H_{6.6}$ZSM-5 samples. Over longer period than 1 day, at room temperature and 400 K the SIMPLISMA analysis does not provide supplementary results with respect to the qualitative analysis of the DRUVv results described above.

From the DRUVv experiments, several quantitative findings can be pointed out. The maximum of the $NPH^{\bullet+}$ concentration as well as the ionization rate increase dramatically with the calcination temperature of the zeolite. The amount of $NPH^{\bullet+}$ can reach 15% of NPH loading assuming absorption coefficient values analogous to those reported in solution. The maximum of the charge separated state (CSS) concentration was observed to increase dramatically with the $NPH^{\bullet+}$ yield. In contrast, the maxima of $NPH^{\bullet+}$ and CSS concentrations increase with the aluminum content of the zeolite ($n = 3.4, 6.6$) and the NPH loading. These trends were analogous to the results deduced from EPR experiments, Table 1.

Raman Scattering Study of Naphthalene Sorption in Calcined H_nZSM-5 Zeolites. The sorption process of NPH in H_nZSM-5 ($n = 0, 3.4, 6.6$) zeolites at loading corresponding to 1, 2, and 4 NPH per unit cell was monitored as a function of time using both FT-Raman spectrometry with exciting wavelength at 1064 nm and dispersive Raman technique with excitation wavelength at 632.8 nm

The data processing using the SIMPLISMA approach of all the FT-Raman spectra recorded over several weeks in the mid-frequency region during the sorption in siliceous ZSM-5 or silicalite-1 provides evidence of one Raman spectrum. This spectrum was identical to Raman spectrum of NPH in solution. In the same way, the analysis of spectra sets obtained during the sorption of NPH in acidic H_nZSM-5 ($n = 3.4, 6.6$) dehydrated under Ar provides evidence for two Raman spectra. The first one was straightforward assigned to residual bulk NPH and the second one with a prominent band centered at 1612 cm^{-1} was assigned to NPH occluded in close proximity to H^+ cation. The reconstructed spectra obtained from the resolved spectra of individual species were in agreement with the experimental spectra. Residuals are reasonably small and have a random pattern. Associated parameter was less than 0.05 (see Experimental Section).

The modeling of the preferred location of NPH in the void space of H_nZSM-5 zeolites performed using Monte Carlo simulation and subsequent energy minimization indicate the close proximity of NPH with −OH group in the straight channel, Figure 7 (see Experimental Section). These results are in accurate agreement with X-ray diffraction study.[22]

The SIMPLISMA procedure was also carried out with FT-Raman spectra set recorded over two weeks after the mixture of the solid NPH with H_nZSM-5 ($n = 3.4$) activated under O_2 at 773 K. This analysis yields three typical spectra exhibited in Figure 8 a−c.

The residual NPH was identified by direct comparison with the Raman spectrum of NPH in bulk state, Figure 8a. The second one that displays narrow lines at 1257, 1329, 1410, 1481, 1520, 1550, and 1597 cm^{-1} was unknown, Figure 8b. The third one displays a prominent broad band centered at 1612 cm^{-1} and was analogous to the spectrum obtained in the same zeolite dehydrated under Ar (see above), Figure 8c. The Raman spectrum of $NPH^{\bullet+}$ is not extracted from spectra set recorded with exciting wavelength at 1064 nm. The concentration of $NPH^{\bullet+}$ was assumed to be too low to be observed in off resonance conditions taking into account the poor Raman cross section of the vibrational modes with 1064 nm exciting wavelength.

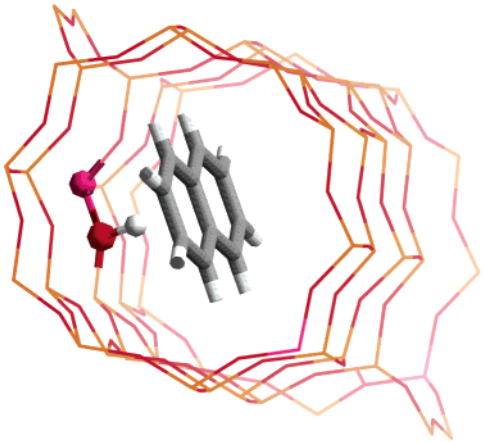

Figure 7. Modeling of the structure of NP occluded in the straight channel of HZSM-5 zeolite. Yellow and red sticks represent the Si and O atoms of the framework, respectively. Pink, red, and white balls represent the Al, O, and H atoms of the Al−O−H group of the framework. Light and dark gray cylinders represent the H and C atoms, respectively.

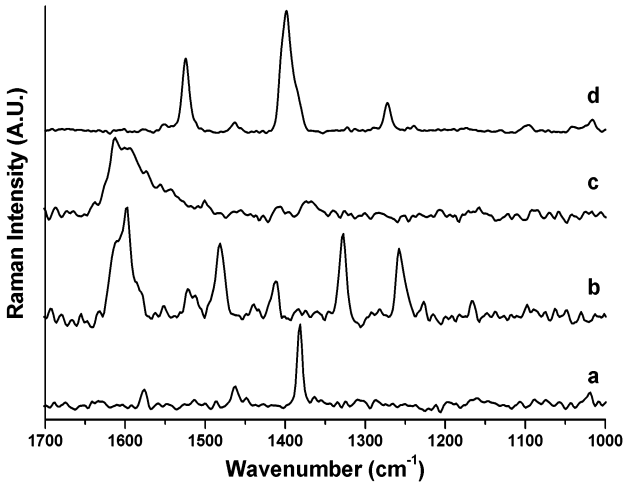

Figure 8. Pure Raman spectra extracted using the SIMPLISMA method of the FT Raman data recorded during the sorption of naphthalene into $H_{3.4}(AlO_2)_{3.4}(SiO_2)_{92.6}$ (a) solid naphthalene, (b) NPH close to the electron−hole pair, (c) NPH occluded close to OH groups, and (d) Resonance Raman spectrum of $NPH^{\bullet+}$ (exciting wavelength, λ = 632.8 nm).

Resonance Raman (RR) scattering spectra were carried out using the 632.8 nm exciting laser line within the visible absorption bands of $NPH^{\bullet+}$. Many Raman spectra were recorded at room temperature over two weeks after the mixture of the solid NPH and $H_nZSM\text{-}5$ (n = 3.4) activated under O_2 at 773 K. In the resonance conditions, only one spectrum type was obtained during the period and is shown in Figure 8d. The resonance Raman bands were analogous in wavenumber and relative intensities to those previously reported in glassy matrix at 77 K for $NPH^{\bullet+}$ with 640, 610, and 605 nm excitation wavelengths.[41] The resonance effect enhances particularly the Raman scattering intensity of three lines observed at 1272, 1398, and 1524 cm^{-1} in spectrum 8d. The 1015, 1524, 2031, and 2538 cm^{-1} RR lines were assigned to second, third, fourth, and fifth harmonics of the 507 cm^{-1} mode, respectively. The resonance effect is specific of $NPH^{\bullet+}$ and the other species exhibit very weak Raman intensities. The wavenumber values and relative intensities of RR spectrum of occluded $NPH^{\bullet+}$ in zeolite and RR spectrum of trapped $NPH^{\bullet+}$ in glassy matrix were very similar. This finding indicates weak effect of the electrostatic field in the straight channel of zeolite upon the vibrational and electronic properties of $NPH^{\bullet+}$.

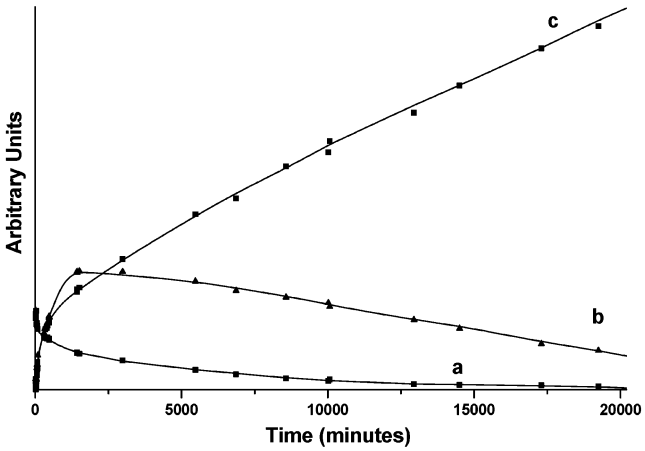

Figure 9. Relative contribution as a function of time of pure species deduced by the SIMPLISMA method from FT-Raman spectra recorded during the sorption of naphthalene into $H_{3.4}(AlO_2)_{3.4}(SiO_2)_{92.6}$: (a) solid naphthalene (NPH), (b) NPH close to the electron−hole pair, (c) NPH occluded close to OH groups.

All the results obtained after Raman scattering investigations of the NPH sorption in $H_nZSM\text{-}5$ (n = 6.6) exhibited analogous trends with those shown above for $H_nZSM\text{-}5$ (n = 3.4).

Figure 9 exhibits the relative amounts of species corresponding to the extracted spectra exhibited in Figure 8a−c as a function of time during 15 days after the mixture of NPH with $H_nZSM\text{-}5$ (n = 3.4) activated under O_2 at 773 K. Curve 9a exhibits the continuous decrease of solid NPH amount, while curve 9c indicates the continuous increase of NPH occluded in the vicinity of H^+. The amount of unknown species, Figure 9b corresponding to FT-Raman spectrum of Figure 8b, was maximum 24 h after the mixing of solids and was relatively stable over the 15 following days. This spectrum does not exhibit any vibrational characteristics of $NPH^{\bullet+}$ and does not resemble any expected spectrum to our knowledge. However, the variation of amount of such species as a function of time is analogous to those observed for the so-called electron−hole pair detected by EPR or UV−visible absorption. These findings lead us to assume that the unknown Raman spectrum corresponds to NPH in close proximity to electron−hole moiety in the void space of zeolites, Figure 8b.

Chemical Extraction of Occluded Species Derived from Naphthalene Sorption in Calcined $H_nZSM\text{-}5$ Zeolites. To characterize the nature of stable occluded products derived from NPH sorption into zeolites, the zeolite frameworks of several typical samples were destroyed by chemical means (see Experimental Section) and the resulting residues were extracted by chloroform. According to the chromatography experiments, NPH is the unique stable species to be extracted and there is no evidence of either polycyclic aromatic compounds such as "coke" or monocyclic compound like benzene.

SECSY and HYSCORE Measurements of Intermediates Generated during Naphthalene Sorption in Calcined $H_nZSM\text{-}5$ Zeolites. Pulse EPR experiments were performed to obtain a detailed picture of the chemical environment of spins generated during the primary spontaneous ionization (Figure 10) and subsequent formation of electron−hole moieties (Figure 11). Both joined two pulse spin−echo correlation spectroscopy (SECSY) and hyperfine sublevel correlation spectroscopy (HYSCORE) experiments were carried out at room temperature and at 4.2 K. In a first step, these experiments were carried out during the primary spontaneous ionization of NPH, Figure 10.

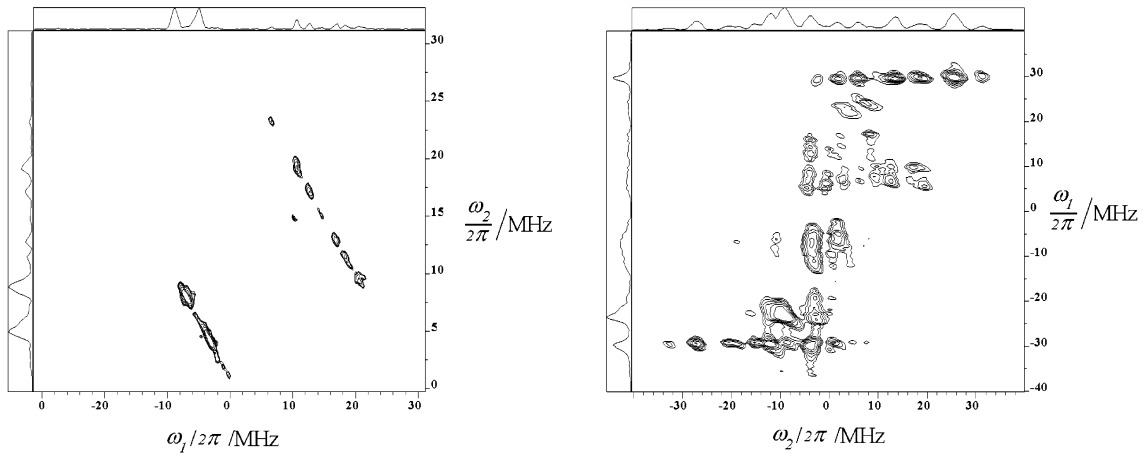

Figure 10. HYSCORE spectrum (left) and 2-pulses SECSY spectrum (right) of $NPH^{\bullet+}$ occluded in H_3ZSM-5 zeolite calcined under oxygen. The spectra were recorded at 4.2 K. HYSCORE spectrum was achieved with a $\tau = 256$ ns and pulse lengths of 12 ns for $\pi/2$ pulses and 24 ns for π pulse were used and a four-step phase cycling ($\pi/2-\tau-\pi/2-t_1-\pi-t_2-\pi/2-\tau-$echo) was applied to suppress unwanted echo. 2-Pulses SECSY spectrum was achieved with pulse lengths of 12 ns for $\pi/2$ pulses and a 16-step phase cycling ($\pi/2-t_1-\pi/2-t_1t_2-$echo) was applied.

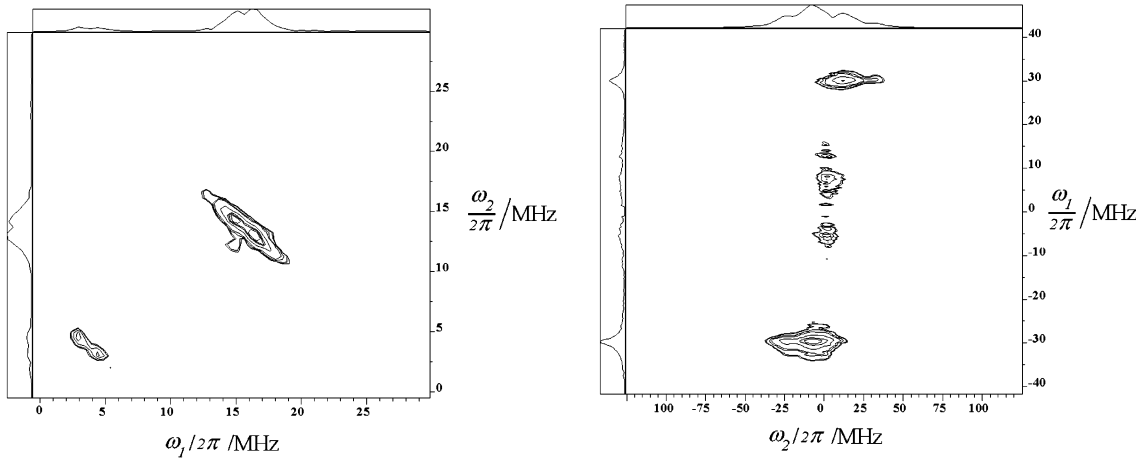

Figure 11. HYSCORE spectrum (left) and 2-pulse SECSY spectrum (right) naphthalene electron species occluded in H_3ZSM-5 zeolite calcined under oxygen. The spectra were recorded at 4.2 K at the maximum of CW EPR signal. HYSCORE spectrum was achieved with a $\tau = 256$ ns and pulse lengths of 12 ns for $\pi/2$ pulses and 24 ns for π pulse were used and a four-step phase cycling ($\pi/2-\tau-\pi/2-t_1-\pi-t_2-\pi/2-\tau-$echo) was applied to suppress unwanted echo. 2-Pulses SECSY spectrum was achieved with pulse lengths of 12 ns for $\pi/2$ pulses and a 16-step phase cycling ($\pi/2-t_1-\pi/2-t_1t_2-$echo) was applied.

This chemical situation was obtained on sample obtained 1 day after the mixing of solid NPH with H_3ZSM-5 calcined at 773 K under O_2 (see Experimental Section). The CW EPR spectrum of this sample is characterized by the proton hyperfine splitting of $NPH^{\bullet+}$ overlapped on a broad signal attributed to unpaired electron (see the CW EPR paragraph). SECSY is a reliable technique that can be used for studying nuclear modulation pattern. The collection of the echo shape at the top of echo peak for each t_1 as function of t_2 leads to record CW spectrum along f_2 domain after Fourier transform procedure.

We show in Figure 10 (right) of SECSY 2D contour plot the double frequency of nuclear modulation from matrix protons which appeared along f_1 domain in both positive and negative quadrants at the nuclear Zeeman frequency $\omega_H/2\pi = 29$ MHz covering 30 MHz along the t_2 CW domain spectra. This result is close to the maximum A_x component of the hyperfine tensor measured of -24.1 MHz of the 1, 4, 5, and 8 protons in the CW naphthalene cation radical previously published.[31] The $\omega_H/2\pi = 29$ MHz observed results from the combination lines. The 2D SECSY spectrum also depicts on the f_1 negative quadrant a peak centered at ^{13}C nuclear Zeeman frequency of 3.7 MHz with a very weak contribution around 0 MHz. On the positive quadrant, another peak is observed at 7.4 MHz that can be attributed to the number of carbon $I = 1/2$ coupled with the spin $S = 1/2$. Moreover, on the negative quadrant additional ^1H pattern around 25 MHz is also observed resulting from Heisenberg spin exchange process from the weak coupled hydrogen 2,3,6,7 with the hydrogen 1,4,5,8. The corresponding HYSCORE spectrum with a τ value of 256 ns displays a strong ^1H modulation pattern with an anisotropic constant of 14 MHz (Figure 10, left). This observed anisotropic coupling constant is close to those found for the proton 1,4,5,8 for the A_z component of -17.4 MHz.[31] On the negative quadrant ω_1 frequency domain nuclear frequency ^{13}C is detected at 3.7 MHz and the double quantum $2\nu^{13}C$ is present in the spectrum. These findings provided further information to previous electron nuclear double resonance (ENDOR) and electron spin−echo envelope modulation (ESEEM) results concerning $NPH^{\bullet+}$ photogenerated in H-ZSM-5 and $CFCl_3$ matrix at low temperature.[31] Interactions of unpaired electron of $NPH^{\bullet+}$ with ^1H of diaromatic moiety were demonstrated in the previous and present works. The present SECSY and HYSCORE results demonstrate supplementary interactions between trapped electron and ^{13}C of $NPH^{\bullet+}$. The two paramagnetic species formed primary after sorption of NPH in H_nZSM-5 ($n = 3.4, 6.6$) interact differently with the surrounding ^{13}C and ^1H magnetic nuclei. However,

no evidence was found for interaction of trapped electron with ^{29}Si or ^{27}Al.

Comparatively, the SECSY and HYSCORE spectra recorded on the broad line of CW electron EPR spectrum assigned to electron−hole pairs show drastic change of the nuclear pattern. This chemical situation was represented by a sample obtained 1 month after the mixing of solid NPH with H_3ZSM-5 calcined at 773 K under O_2 (see Experimental Section) and the complete disappearance of the proton hyperfine splitting of $NPH^{\bullet+}$ in the CW EPR spectrum. The 2D SECSY contour plot shows in both positive and negative f_1 quadrants the double quantum peak of ^{13}C nuclear modulation (7.4 MHz) centered at 0 MHz in the f_2 domain (Figure 11, right). This is consistent with isolated electrons coupled with ^{13}C. In addition, the combination lines 2ν ^{1}H pattern of 29 MHz in the f_1 domain are centered at the carbon nuclear frequency, 7.4 MHz, in the f_2 domain. Such change were also observed in the HYSCORE spectrum where the ^{1}H anisotropic constant is decreased from 14 MHz (Figure 10, left) to 7 MHz (Figure 11, left) and a weak carbon coupling is observed in the (+,+) f_2 domain with an anisotropic constant of 3.5 MHz and a positive sign for hyperfine splitting constant (Figure 11, left). Moreover, no signal feature from zeolite interaction through ^{29}Si or ^{27}Al was observed in the HYSCORE spectrum. The same patterns of HYSCORE and SECSY are observed for room temperature and 4.2 K measurements so the 3.7 MHz pattern observed in the HYSCORE spectrum cannot be attributed to ^{27}Al nucleus for which nuclear modulation frequency are closed from ^{13}C one. Such results seem to indicate that the unpaired electrons of electron−hole pair are surrounding but remain close to the occluded neutral NPH. No evidence of ^{29}Si and ^{27}Al interactions was found. In contrast, from previous pulse EPR results concerning sorption of biphenyl in identical zeolites the unpaired electrons of electron−hole pairs were coupled with ^{29}Si and ^{27}Al nuclei of zeolites.

Discussion

UV−visible absorption and Raman scattering results obtained during the investigations of the sorption of NPH in Al-free ZSM-5 zeolite ($n = 0$) calcined under O_2 or Ar provide evidence of neutral NPH occluded in the void space of ZSM-5 after several weeks of exposure of solid NPH to empty zeolite at room temperature. Analogous results were obtained during the investigations of the sorption of NPH in H_nZSM-5 zeolite ($n =$ 3.4, 6.6) gently dehydrated under Ar. All these results agree with that of previous works in NPH/ZSM-5 systems.[22] The preferred adsorption site is at the intersections of straight and sinusoidal channels. Compared to the empty framework, the straight channel pores in loaded ZSM-5 are strongly elliptically deformed while the sinusoidal channel pores are hardly affected by the sorption of NPH.

In contrast, when the aluminated acidic H_nZSM-5 zeolites ($n = 3.4$, 6.6) are calcined under O_2 above 573 K, EPR, UV−visible absorption, and Raman scattering results provide evidence of supplementary species. The primary observed process is the spontaneous electron abstraction of NPH to produce radical cation $NPH^{\bullet+}$ and the important related problem is the nature of the trapping sites of the empty zeolite generated by the thermal treatment under O_2. It was possible to establish that this primary reaction is not initiated by oxidizing impurities but catalyzed by LAS rather than by BAS. LAS are essentially electron acceptor centers. The origin of LAS of aluminated H_n-ZSM-5 zeolites created by the calcination under O_2 is still controversial. Precise control and definition of the calcination conditions was an important requirement for the implementation of reproducible experiments. One way to specifically probe the efficiency of active LAS was the application of IR spectroscopy in conjunction with the sorption of pyridine. Less than 0.4/UC of LAS was detected after calcination under O_2 whereas the LAS amount was very low after gentle calcination under Ar. The LAS are not thought to be inherent to the ZSM-5 structure but probably result in partial breaking of Al−O bands.[29] The LAS amount increases slightly with increase of temperature of calcination. However, no noticeable influence on the local structure of framework aluminum atoms was detected.[42] The low amount of extraframework aluminum species did not generate noticeable effect upon LAS amount.

The NPH exhibits gas-phase ionization potential value of 8.14 eV in gaseous phase and its sorption into activated H_nZSM-5 ($n = 3.4$, 6.6) zeolites probes the electron acceptor ability of LAS. It was found through the EPR and UV−visible results that the maximum yield of $NPH^{\bullet+}$ (Table 1) increases gradually as the temperature of thermal treatment under O_2 increases, namely, from 573 to 973 K for H_nZSM-5 ($n = 3.4$, 6.6). The ionization yield of NPH increases slightly when the aluminum content increases from 3.4 Al to 6.6 Al. The NPH ionization yield values listed in Table 1 correlate accurately with LAS amount but do not correlate with the quantity of extraframework aluminum species. The $NPH^{\bullet+}$ amounts are markedly higher than the estimated quantities of LAS and extraframework species.

The sorption process provokes the uptake of NPH at the pore openings of zeolite microcrystals and the simultaneous ionization occurs through abstraction of electron by the electron acceptor LAS in the inner surface. In general, the ionization energy, I_e of molecules in condensed phase is represented by $I_e = I_g + P_+ + V_0$ where P_+ is the polarization energy of the surrounding, $I_g = 8.14$ eV is the NPH ionization potential in the gas phase, and V_0 is the conduction band energy in the condensed phase.[43] The high polarization energy P_+ of NPH occluded in the straight channel in close proximity of LAS induces probably spontaneous ionization (CS) by lowering the ionization energy. The polarization energy P_+ of the surrounding occluded NPH without LAS is too low to generate spontaneous CS. The tight fit between the shape of the $NPH^{\bullet+}$ and the pore size of straight channels of zeolites combined with efficient electron-trapping site appeared the most important factors responsible for the generation and the stabilization of the CS of NPH in $NPH^{\bullet+}$ and trapped electron. This assumption was supported by recent results concerning the role of sorbate size and the prevalence of internal surface of void space on spontaneous ionization yield.[44] Observation of $NPH^{\bullet+}$ indicates spontaneous ET reaction between occluded NPH and zeolite framework. The CW EPR and UV absorption results provide good evidence of both $NPH^{\bullet+}$ and trapped electron. However, in contrast to previous works where unpaired electron of paramagnetic moieties interacts with ^{27}Al nuclei of zeolite, the present pulsed EPR results obtained at room temperature provide no evidence of interaction between trapped electron and magnetic nuclei of host.[13] Unfortunately, the pulse EPR results do not provide any structural information about the trapping site of the ejected electron within the zeolite framework in the primary sorption process.

Observation of the complete disappearance as a function of time of $NPH^{\bullet+}$ with the persistence of paramagnetic species in high yield indicates that a supplementary ET reaction between $NPH^{\bullet+}$ and zeolite framework is taking place during the migration of $NPH^{\bullet+}$ and trapped electron in the void space. The

identification of NPH in the ground state by Raman scattering as well as identification of isolated electron at 0 MHz in SECSY experiment supported the assumption of positive holes. The occurrence of the ET reaction is not surprising considering results recently reported demonstrating ET from zeolite to other powerful electron acceptors such as chloranyl, cyano substituted benzene molecules, and biphenyl radical cation.[13,32,45] The ZSM-5 zeolite participates as an electron donor in ET reaction with occluded $NPH^{\bullet+}$ preferentially to the direct charge recombination with trapped electron. A possible source of electron density for electron donation to $NPH^{\bullet+}$ is the lone pair of electrons on the bridging lattice oxygen atoms, particularly those in $[Si-O-Al]^-$ sites. The spontaneous initial CS evolves to long-lived CSS as an electron−hole pair. Considering the EPR results alone, we are not able to exclude the presence of coke as previously reported for other systems.[11] However, the unique stable polyaromatic species detected after the breakdown of the zeolite framework was naphthalene (NPH). The experimental results suggest that both electron and hole migration can occur between electron donors and acceptors spatially separated and concerted with the migration of NPH within the straight channel of zeolite. It is difficult to estimate the mean electron−hole distance from the present experimental results; however, comparison with analogous results with biphenyl indicates location of electron and hole in close proximity of the straight channel containing occluded NPH. For instance, during the migration of NPH along the straight channel, the hole may move along electron-rich framework sites such as oxygen atoms within $[Si-O-Al]^-$ while the electron may move along electron-deficient sites of aluminum centers.

After the uptake of NPH by pore opening, the fast initial CS between $NPH^{\bullet+}$and electron-trapping site E^- generated by LAS occurs:

$$NPH_0^{\bullet+} \square E_0^-$$

where $\square$ represents the void space of the straight channel.

Then, electron abstraction by $NPH^{\bullet+}$ from zeolite occurs and generates CSS as electron (E^-) and positive hole (D^+) and regenerates LAS. The formation of long-lived CSS was due to the effective hole and electron migration concerted with the NPH diffusion to efficient trapping sites:

$$D_0^+ \square NPH_0 \square E_0^- \leftrightarrow D_1^+ \square NPH_1 \square E_1^- \leftrightarrow ... \leftrightarrow D_i^+ \square NPH_i \square E_i^-$$

The deactivation of the long-lived CSS appears to be regulated by the long distance back-electron-transfer process to regenerate occluded NPH in ground state:

$$\square NPH_0 \square \leftrightarrow \square NPH_1 \square \leftrightarrow ... \leftrightarrow \square NPH_i \square$$

The ionization yields of NPH were higher than ones obtained with biphenyl with identical thermal treatment of the zeolites. This comparison indicates that the NPH ionization yield ($NPH_0^{\bullet+} \square E_0^-$) is markedly higher than LAS one and it is probable that the ionization occurs through a catalytic pathway. In the same way, the electron−hole pair ($D_i^+ \square NPH_i \square E_i^-$) yields were higher than ($NPH_0^{\bullet+} \square E_0^-$) ones. A new catalytic redox pathway is probably involved. The deactivation of the long-lived CSS occurs over a long period at room temperature. The stable state is diamagnetic neutral naphthalene occluded in the pores of ZSM-5 zeolite. The deactivation period will be shortened by gentle warming of the sample.

Acknowledgment. The authors are very grateful to Dr. J. Patarin for providing ultrapure quality zeolites and to B. Sombret for assistance and advice while using FT-Raman spectrometry. The Centre d'Etudes et de Recherches Lasers et Applications (CERLA, FR-CNRS 2416) is supported by the Ministère chargé de la recherche, the région Nord/Pas de Calais, and the Fonds Européen de Développement Economique des Régions.

References and Notes

(1) Hagfeld, A.; Grätzel, M. *Acc. Chem. Res*. **2000**, *33*, 269.
(2) Turro, N. J.; Lei, X.; Li, W.; Liu, Z.; McDermott, A.; Ottaviani, M. F.; Abrams, L. *J. Am. Chem. Soc*. **2000**, *122*, 11649.
(3) Thomas, J. K. *Chem. Rev*. **1993**, *93*, 301.
(4) Yoon, K. B. *Chem. Rev*. **1993**, *93*, 321.
(5) Ramamurthy, V.; Lakshminarasimhan, P.; Grey, C. P.; Johnston, L. J. *Chem. Commun*. **1998**, 2411.
(6) Stamires, D. N.; Turkevich, J. *J. Am. Chem. Soc*. **1964**, *86*, 749.
(7) Chen, F. R.; Fripiat, J. J. *J. Phys. Chem. B* **1993**, *97*, 5796.
(8) Cozens, F. L.; Bogdanova, R.; Régimbald, M.; Garcia, H.; Marti, V.; Scaino, J. C. *J. Phys. Chem. B* **1997**, *101*, 6921.
(9) Garcia, H; Roth, H. D. *Chem. Rev*. **2002**, *102*, 3947.
(10) Kiricsi, I.; Förster, H.; Tasi, G.; Nagy, J. B. *Chem. Rev*. **1999**, *99*, 2109.
(11) Hunger, M.; Weitkamp, J. *Angew. Chem., Int. Ed*. **2001**, *40*, 2954.
(12) Gener, I.; Moissette, A.; Brémard, C. *Chem. Commun*. **2000**, 1536.
(13) Moissette, A.; Vezin, H.; Gener, I.; Patarin, J.; Brémard C. *Angew. Chem., Int. Ed*. **2002**, *41*, 1241.
(14) Windig, W.; Guilment, J. *J. Anal. Chem*. **1991**, *63*, 1425.
(15) Windig, W.; Antalek, B.; Lippert, J. L.; Batonneau, Y.; Brémard, C. *Anal. Chem*. **2002**, *74*, 1371.
(16) Moissette, A.; Batonneau, Y.; Brémard, C. *J. Am. Chem. Soc*. **2001**, *123*, 12325.
(17) Moissette, A.; Gener, I.; Brémard, C. *J. Phys. Chem*. B **2001**, *105*, 5647.
(18) Yakushi, K.; Ikemoto, I.; Kuroda, H. *Acta Crystallogr., Sect. B* **1973**, *29*, 264.
(19) Van Koningsveld, H.; Jansen, J. C.; Van Bekkum, H. *Zeolites* **1990**, *10*, 235.
(20) Van Koningsveld, H. *Acta Crystallogr*. **1990**, *B46*, 731.
(21) Van Koningsveld, H.; Van Bekkum, H.; Jansen, J. C. *Acta Crystallogr*. **1987**, *43B*, 127.
(22) Van Koningsveld, H.; Janssen, J. C. *Microporous Mater*. **1996**, *6*, 159.
(23) Grau-Crespo, R.; Peralda, A. G.; Ruiz-Salvador, A. R.; Gomez, A.; Lopez-Cordero, R. *Phys. Chem. Chem. Phys*. **2000**, *2*, 5716.
(24) Schüth, F.; Althoff, R. *J. Catal*. **1993**, *143*, 388.
(25) Smirnov, K. S.; Tsyganenko. A. A. *Chem. Phys. Lett*. **1991**, *182*, 127.
(26) Bludau, H.; Karge, H. G.; Niessen, W. *Microporous Mesoporous Mater*. **1998**, *22*, 297.
(27) Costa, C.; Dzikl, I. P.; Lopes, J. M.; Lemos, F.; Ribeiro, F. R. *J. Mol. Catal. A* **2000**, *154*, 193.
(28) Catana, G.; Baetens, D.; Mommaerts, T.; Schoonheydt, R. A.; Weckhuysen, B. M. *J. Phys. Chem. B* **2001**, *105*, 4904.
(29) Woolery, G. L.; Kuehl, G. H.; Timken, H. C.; Chester, A. W.; Vartuli, J. C. *Zeolites* **1997**, *19*, 288.
(30) Goldfarb, D.; Bernardo, M.; Strohmaier, K. G.; Vaughan, D. E. W.; Thomann, H. *J. Am. Chem. Soc*. **1996**, *116*, 6344.
(31) Erickson, R.; Benetis, N. P.; Lund, A.; Lingren, M. *J. Phys. Chem*. **1997**, *101*, 2390.
(32) Samoilova, R. I.; Shubin, A. A.; Bowman, M. K.; Hûttermann, J.; Dikanov, S. A. *Chem. Phys. Lett*. **2000**, *316*, 404.
(33) Gener, I.; Moissette, A.; Vezin, H.; Patarin, J.; Brémard, C. *Stud. Surf. Sci. Catal*. **2001**, *135*, 2272.
(34) Cherisov, S. D.; Trifunac, A. D. *Chem. Phys. Lett*. **2001**, *347*, 65.
(35) Andrews, L.; Kelsall, B. J.; Blankenship, T. A. *J. Phys. Chem*. **1982**, *86*, 2916.
(36) Kelsall, B. J.; Andrews, L. J. *Chem. Phys*. **1982**, *76*, 5005.
(37) Andrews, L.; Blankenship, T. A. *J. Am. Chem. Soc*. **1981**, *103*, 5977.
(38) Gener, I.; Buntinx, G.; Brémard, C. *Angew. Chem., Int. Ed*. **1999**, *38*, 1819.
(39) Tsuchida, A.; Tsujii, Y.; Ito, S.; Yamamoto, M. *J. Phys. Chem*. **1989**, *93*, 1244.

(40) Badger, B.; Brocklehurst, B. *Trans. Faraday Soc.* **1969**, *65*, 2588.
(41) Kawashima, H.; Kato, T.; Shida, T. *Chem. Phys. Lett*. **1990**, *165*, 59.
(42) Seiler, M.; Wang, W.; Hunger, M. *J. Phys. Chem. B* **2001**, *105*, 8143.
(43) Hirata, Y.; Mataga, N. *Prog. React. Kinet*. **1993**, *18*, 273.
(44) Moissette, A.; Marquis, S.; Gener, I.; Brémard, C. *Phys. Chem. Chem. Phys.* **2002**, *4*, 5690.
(45) O'Neill, M. A.; Cozens, F. L.; Schepp, N. P. *J. Phys. Chem. B* **2001**, *105*, 12746.